applied sciences

MDPI

Article

"Migrate-Transfer-Control" Support System of Surrounding Rock in the Deep Roadway and Its Application

Tao Qin [1,2], Binyang Duan [1,2], Yanwei Duan [1,3,*], Yaozu Ni [1,2], Xiangang Hou [1,2], Pingyun Ma [1,2] and Yue Yang [4]

[1] Key Laboratory of Mining Engineering of Heilongjiang Province College, Heilongjiang University of Science and Technology, Harbin 150022, China
[2] College of Mining Engineering, Heilongjiang University of Science and Technology, Harbin 150022, China
[3] College of Safety Engineering, Heilongjiang University of Science and Technology, Harbin 150022, China
[4] College of Civil Engineering, Heilongjiang University of Science and Technology, Harbin 150022, China
* Correspondence: duan_yanwei@126.com

Abstract: After coal mining enters the deep, the mining environment changes dramatically, and engineering disasters become increasingly prominent, which are mostly related to rock instability and failure. As traditional support is difficult to meet production needs, it is necessary to improve the support system. Based on the engineering background of the Pinggang mining roadway, this work studies the migration law of overlying strata in deep goaf by theoretical analysis and numerical simulation. The results show that the vertical stress and plastic failure range of the surrounding rock in front of the working face increase with the advance distance and when the working face advances to the first square, reaching the maximum. A stope spatial model considering the influence of horizontal stress is established. Combined with the theory of key strata, the stress transfer characteristics of overlying strata are analyzed. It can be seen that 0~30 m in front of the coal wall of the working face is the influence range of advanced abutment pressure, and the dynamic mining pressure in this range has a great influence. The inclined direction of the working face, 0~20 m away from the coal wall of the roadway, is the influence range of the solid coal abutment pressure. On this basis, the "migration-transfer- control" technical system of surrounding rock in deep stope face is put forward, i.e., the stress transfer of surrounding rock is caused by overlying rock migration, and the large deformation of surrounding rock is controlled by supporting means. Based on the original support scheme of the roadway, three reinforcement schemes are designed for the roof, the sidewalls, and both the roof and sides. The deformation control effect of the reinforcement scheme is far greater than that of the single factor, and the field monitoring effect is good. The research results aim to provide theoretical and technical support for the deformation control of mining roadways in the deep mining process.

Keywords: deep mining; mining roadway; overburden rock migration; stress transfer; support system

check for updates

Citation: Qin, T.; Duan, B.; Duan, Y.; Ni, Y.; Hou, X.; Ma, P.; Yang, Y. "Migrate-Transfer-Control" Support System of Surrounding Rock in the Deep Roadway and Its Application. *Appl. Sci.* **2023**, *13*, 6325. https://doi.org/10.3390/app13106325

Academic Editor: Tiago Miranda

Received: 7 April 2023
Revised: 9 May 2023
Accepted: 16 May 2023
Published: 22 May 2023

Copyright: © 2023 by the authors. Licensee MDPI, Basel, Switzerland. This article is an open access article distributed under the terms and conditions of the Creative Commons Attribution (CC BY) license (https://creativecommons.org/licenses/by/4.0/).

1. Introduction

China's resource endowment is characterized by "lack of gas, less oil and rich coal", which means that coal will remain the dominant energy source in China for a long time in the future [1,2]. In recent years, in order to meet the economic development, the total energy demand is increasing year by year. To ensure energy supply, the mining of coal resources in Northeast China and East China is advancing at a speed of 10–25 m/a to a depth of 800~1000 m. After entering deep mining, the mining environment changes dramatically [2–4]. The main change is that the ground stress increases evidently, which is caused by the high vertical stress and tectonic stress caused by the weight of overburden rock. Therefore, the safe mining of deep coal resources is a huge challenge [5].

Overburden movement is easy to occur in deep stope under high stress. Mining-induced overburden movement is the root of all mine pressure in the stope, i.e., overburden rock migration causes stress transfer in surrounding rock. Consequently, it has the occasion

to analyze the migration law and stress transfer characteristics of overburdened strata to control the roadway surrounding rock. Regarding the law of overburden rock migration, scholars have proposed many hypothesis models, including the pressure arch hypothesis, the cantilever beam hypothesis, the hinged rock beam hypothesis, the masonry beam hypothesis, and the key stratum theory [6–10]. Taking the key stratum theory as an example, the theory holds that there is a key stratum in the overburden movement, i.e., a certain layer or a few layers of thick and hard rock strata are broken, and then the overburden movement occurs. In terms of stability, the key stratum determines the entire strata. Therefore, the local stability of key strata is the prerequisite for controlling overall stability. This theory illustrates the migration law of overburden rock from the perspective of underground pressure and provides a new idea for coal mine safety mining [11–14]. In view of the key stratum theory, scholars have conducted extensive research and achieved fruitful results. Kong [15] studied the movement and weighting law of overlying strata through theoretical analysis, similar simulation, and field monitoring of an extra-thick coal seam. Kuang et al. [16] analyzed the law of overlying strata movement through in situ investigation, combined with ground monitoring and pressure data, and determined the spatial and temporal relationship between key strata fracture and stope pressure. Zhu et al. [17] analyzed the link between overburden rock movement and roof pressure by studying the motion law of the voussoir beam structure formed by key strata.

The roadway stability is the precondition for safe production. The theory and technology of roadway surrounding rock control have been developed and improved, and many representative surrounding rock control theories have been formed, such as loose circle support theory [18], strength strengthening theory [19], primary and secondary bearing area support theory [20], and key parts coupling support theory [21]. Based on these classical theories, the control technology of roadway surrounding rock has been continuously developed. Based on laboratory tests and energy theory, Xie et al. [22] proposed the supporting principle of accelerating supporting speed and strengthening supporting strength, designed the supporting scheme, and monitored and verified the anchoring force of the bolt. Wang et al. [23] improved the energy support theory and proposed that the energy released in the roadway should be less than the absorbed by the support structure, which was applied to the deep roadway support and achieved good on-site practical results. By analyzing the evolution law of stress from the roadway to surrounding rock, Zuo et al. [24] proposed the theory of equal strength support, i.e., the surrounding rock stress is kept in an equal state by means of pressure relief or support. Kang's team analyzed the characteristics of each stress field in the mine and the relationship between them, and put forward the three-field coupling support principle of "situ stress field, mining stress field and support stress field" and put forward the roadway support–modification–pressure relief cooperative support technology [25–27]. Ma et al. [28] proposed the butterfly theory of plastic zone by analyzing the plastic zone range and used long bolts to reinforce the support. In the study of floor heave control, Zhang et al. [29] pointed out that the roadway is an interactive whole, and the support design should fully consider the overall bearing capacity. Through field test and theoretical analysis, Ren [30] proposed the "three anchors" coupling support technology to carry out deep and shallow grouting of surrounding rock to fully improve the integrity.

The above surrounding rock control technology is only for a certain link or a few links of support, and the study on the whole transfer process of stress is relatively insufficient. Targeting at the current control situation of surrounding rock in Pinggang Coal Mine, this work studies the migration law and stress transfer characteristics of overlying rock in deep goaf and puts forward the technical system of "migrate-transfer-control" of in the deep mining working face. The support scheme is optimized by numerical simulation. After on-site monitoring, the support effect is good. The research results aim to provide theoretical and technical support for the deformation control of mining roadway during deep mining process.

2. Analysis of Surrounding Rock Control Status in Pinggang Coal Mine

Pinggang Coal Mine is located in Jixi City, Heilongjiang Province, China, with a mining area of 35.2 km^2. The surface is hilly and mountainous, and the vertical depth of the working face is 650~680 m. The 33# coal seam has a single coal structure or two layered structures. The middle interlayer of the two layered structure is thin, generally 0.30~1.54 m, which is a mixed layer of shale, tuff shale, and coal shale formation. The coal quality is excellent, bright, massive, and low ash (Ag = 22.47%). The specular coal in the coal seam is medium–wide banded, the stripes are dark black, the physical conditions are good, the curves are well reflected, and the characteristics are evident. Most of the mining area is recoverable, and the coal seam dip angle is 15~30°. The dip angle of the right coal seam is relatively stable, basically 20°. The direct roof of the coal seam is silty fine sand rock with a thickness of 6.0 m. The direct base is shale, and the thickness is 6.2 m.

The roadway of the first right working face of the 33 # coal is a trapezoid. The width × height of the roadway is 4200 mm × 2500 mm. The roof is supported by a bolt, a steel belt, and an anchor cable. There are 4 rows of bolts, and the spacing between bolts is 1000 mm × 1100 mm. The anchor cable in the middle of the roof, and the support density is 3000 mm × 3, as shown in Figure 1.

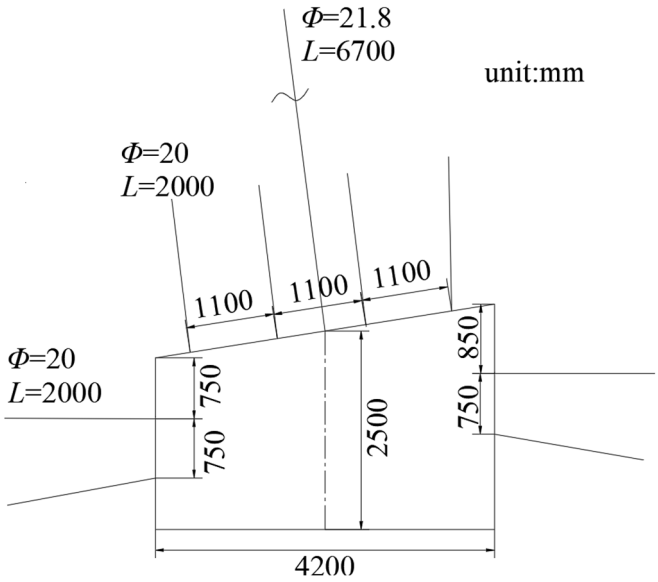

Figure 1. Roadway section support on the first right working face.

According to the field pressure observation, the deformation of the surrounding rock is large, and the metal mesh fracture occurs locally. The amount of floor movement is between 100 mm and 500 mm for 30 days. Through the observation of the roof separation instrument, the amount of roof separation in the first 7 days is generally about 100 mm, and the amount of separation is between 100 mm and 300 mm in 7 days to 30 days.

3. Study on Migration Law of Overlying Strata in Deep Goaf

3.1. Theoretical Analysis of Fracture Instability of Overlying Strata

The mechanical analysis of overburden fracture in goaf is usually simplified into two models: fixed beam and cantilever beam. It is assumed that the length, width, and height of the rock beam are l, b, and h, respectively. The beam is a homogeneous medium and the load is q. The following analysis of two models of rock beam fracture and crack propagation process:

(1) Two-end fixed beam model

Figure 2 is the mechanical model of clamped beam at both ends. Five points are selected on the beam for mechanical analysis, and the selected position is shown in Figure 2a. The mechanical model meets the following requirements:

$$\sigma_{\max} = \frac{M}{W_z} \tag{1}$$

$$\tau_{\max} = \frac{3F_s}{2W_z} \tag{2}$$

$$W_z = \frac{bh^2}{6} \tag{3}$$

where W_z is the bending section coefficient; F_s is bending normal stress; and M is the bending moment.

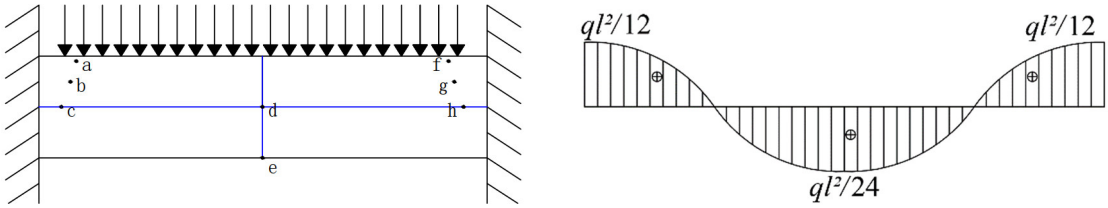

(**a**) (**b**)

Figure 2. Bending moment diagram of clamped rock beam. (**a**) Beam point analysis. (**b**) Fixed rock beam bending moment diagram.

When the maximum stress at both ends $\sigma_{\max}$ > allowable stress $[\sigma]$, cracks began to appear at the end, the stable state was gradually destroyed, the unbalanced force gradually became larger, the cracks developed rapidly, and, finally, the rock beam was destroyed.

Figure 3 is the stress state of each point of the fixed beam. Point a has the maximum normal stress and zero shear stress, which belongs to pure shear failure. As the left and right ends of the rock beam are symmetrical, the stress state of Point f is the same as that of Point a. Point b and Point g have both normal stress and shear stress, which belong to tensile–shear combined failure. Point c and Point h are located on the neutral axis, the normal stress is zero, and the shear stress is the largest, which belongs to shear failure. Point d is the intersection of the neutral axis and the midline, which is not stressed. Point e has only tensile stress, and shear stress is zero, which belongs to shear failure.

As the bending moment at the end is $ql^2/12$, the maximum principal stress can be expressed by Equation (1). The maximum shear stress can be obtained from Equation (2). When the crack propagates downward, Δh, the maximum stress generated at the end is $\sigma' = \frac{ql^2}{2b(h-\Delta h)^2}$. The maximum stress at the end increases and the increment is:

$$\Delta\sigma = \sigma'_{\max} - \sigma_{\max} = \frac{ql^2}{2b(h-\Delta h)^2} - \frac{ql}{2bh^2} \tag{4}$$

where $\Delta\sigma$ is a non-equilibrium force, resulting in accelerated crack propagation.

The generation of cracks on the rock beam is the result of energy release. The released energy is generated by the work, which can be calculated by the stress diagram (see the shaded part in Figure 4). The expression is:

$$J_1 = \int_0^{\Delta h} \frac{ql}{2bh^2} - \frac{ql}{bh^3} y dy = \frac{ql\Delta h}{2bh^2} - \frac{ql\Delta h^2}{2bh^3} \tag{5}$$

$$J_2 = \int_0^{\Delta h} \frac{3ql}{4bh}\left(1 - \frac{4y^2}{h^2}\right)dy = \frac{3ql\Delta h}{4bh} - \frac{4\Delta h^3}{3h^2} \tag{6}$$

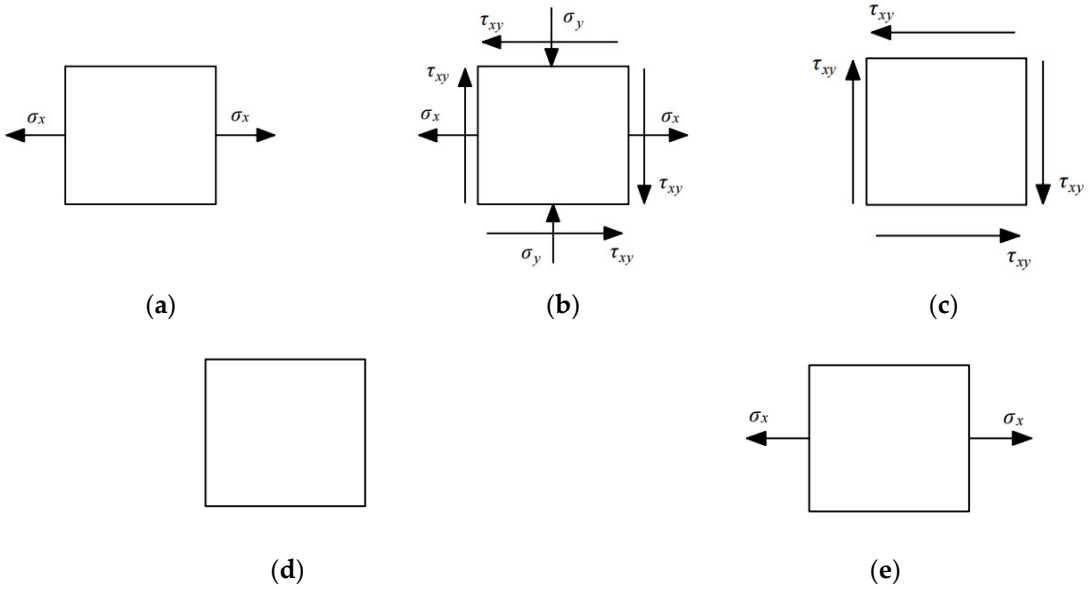

Figure 3. Stress state of each point of the fixed beam. (**a**) Point a. (**b**) Point b. (**c**) Point c. (**d**) Point d. (**e**) Point e.

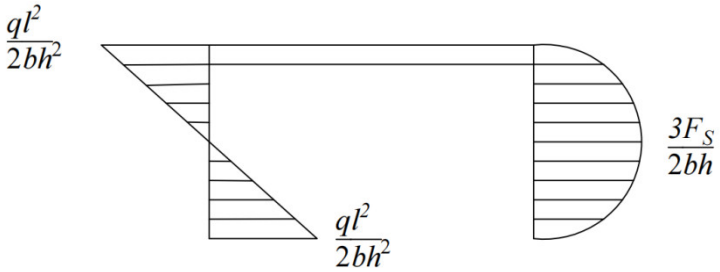

Figure 4. Section of the normal stress and shear stress diagram.

(2) Cantilever beam model

Figure 5 is a schematic diagram of cantilever rock beam. Under the uniform load, the bending moment at the end is the largest, i.e., $M = ql^2/2$, and the following conditions need to be met:

$$\sigma_x = \frac{M_y}{I_z} = \frac{6ql^2y}{h^3} \tag{7}$$

$$\tau = \frac{3F_z}{2bh}\left(1 - \frac{4y^2}{h^2}\right) = \frac{3ql}{2bh}\left(1 - \frac{4y^2}{h^2}\right) \tag{8}$$

Three points on the beam were selected for mechanical analysis, and the specific locations are shown in Figure 6. Figure 7 is the stress state of each point of the cantilever rock beam. Point a had the maximum normal stress and zero shear stress, which belonged to pure shear failure. Point b had both normal stress and shear stress, which belonged to tensile–shear combined failure. Point c was located on the neutral axis, the normal stress was zero, and the shear stress was the largest, which belonged to shear failure.

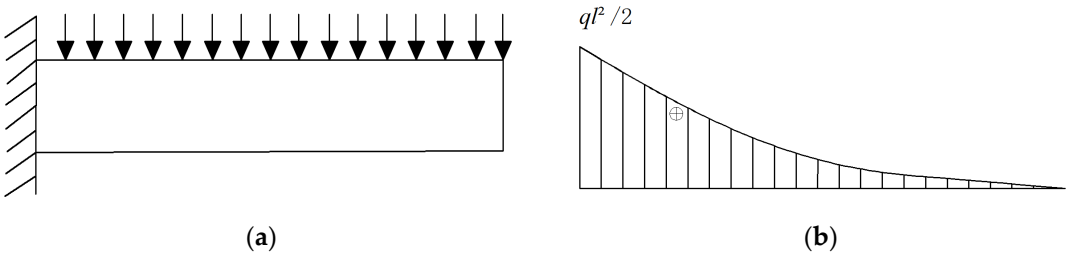

Figure 5. Schematic diagram of cantilever rock beam. (**a**) cantilever rock beam. (**b**) cantilever rock beam bending moment diagram.

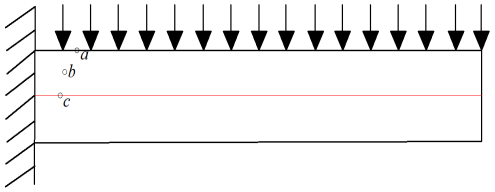

Figure 6. Points on cantilever rock beam.

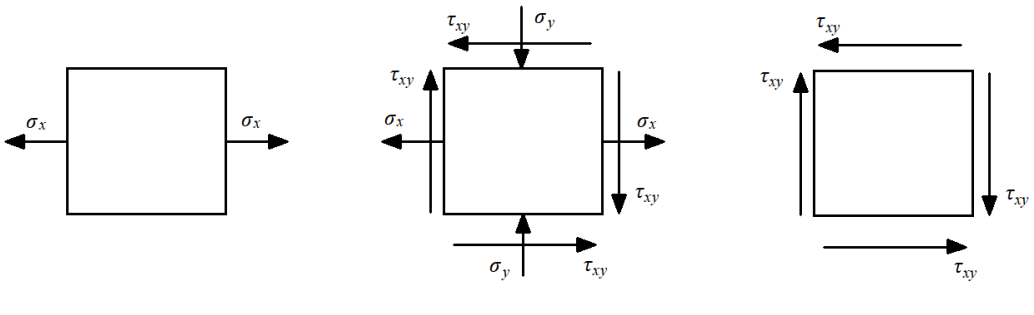

Figure 7. Stress state of each point of cantilever rock beam. (**a**) Point a. (**b**) Point b. (**c**) Point c.

According to Equations (7) and (8), the shear bending moment diagram on the section can be drawn, as shown in Figure 8. At this time, the rock beam is in a stable state. As the load increases, the rock beam begins to crack at the end and gradually destroys. The energy that causes crack propagation (the shaded part in Figure 9) comes from normal stress and shear stress, which can be expressed as

$$J_3 = \int_0^{\Delta h} \frac{3ql^2}{h^2} - \frac{6ql^2}{h^3} y dy = \frac{3ql^2\Delta h}{h^2} - \frac{3ql^2\Delta h}{h^3} \tag{9}$$

$$J_4 = \int_0^{\Delta h} \frac{3ql}{2bh}\left(1 - \frac{4y^2}{h^2}\right) dy = \frac{3ql\Delta h}{2bh} - \frac{2ql\Delta h^3}{bh^3} \tag{10}$$

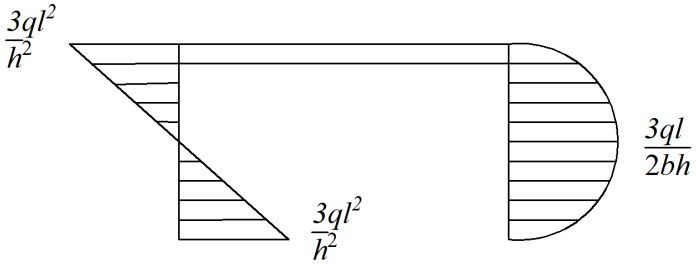

Figure 8. Shear moment diagram on section.

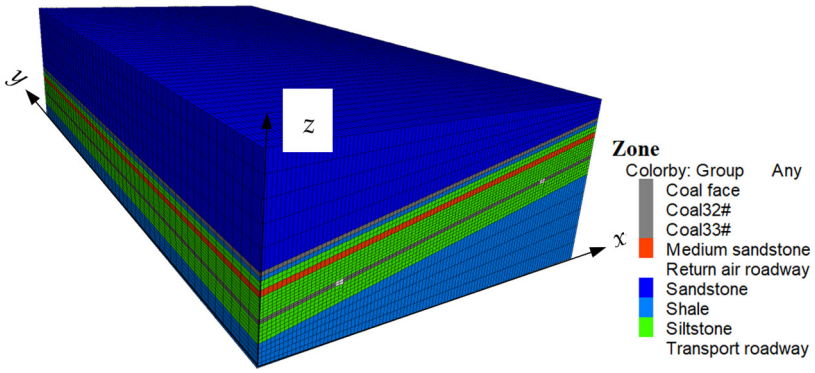

Figure 9. Numerical simulation model.

3.2. Simulation Analysis of Overlying Strata Migration in Goaf

3.2.1. Numerical Model Establishment and Parameter Selection

According to the geological background of the first right working face, a numerical calculation model was established, and the in situ stress of the original rock was the geostatic field type. The size of the model was x × y × z = 200 m × 400 m × 93 m. Considering the influence of calculation accuracy and calculation speed, the model had a total of 834,360 elements and 564,520 nodes. The numerical simulation model is shown in Figure 9.

The model adopted the Mohr–Coulomb constitutive model, the top surface was subjected to the equivalent gravity load, and the surrounding and bottom surfaces were subjected to displacement constraints. The lithology parameters of each rock stratum are shown in Table 1.

Table 1. Main mechanical parameters of rock strata.

Strata	Density/kg·m^{-3}	Bulk Modulus/GPa	Shear Modulus/GPa	Cohesion/MPa	Internal Friction Angle/(°)	Tensile Strength/MPa
Medium sandstone	2530	7.02	4.54	2.62	36	3.01
siltstone	2630	8.21	4.21	3.21	38	4.5
sandstone	2540	6.95	4.42	2.68	33	3.65
32 # coal seam	1440	1.88	1.22	1.90	23	1.65
33 # coal seam	1440	1.88	1.22	1.90	23	1.65
Shale	2430	3.42	1.72	2.11	30	2.3

3.2.2. Overburden Rock Migration Law

(1) Vertical stress distribution characteristic under different advancing distance

To study the development process of overburden rock migration law, the vertical stress cloud map during the working face advancing was first analyzed. It was found that the vertical stress range expanded with the continuous advance, as shown in Figure 10a–k.

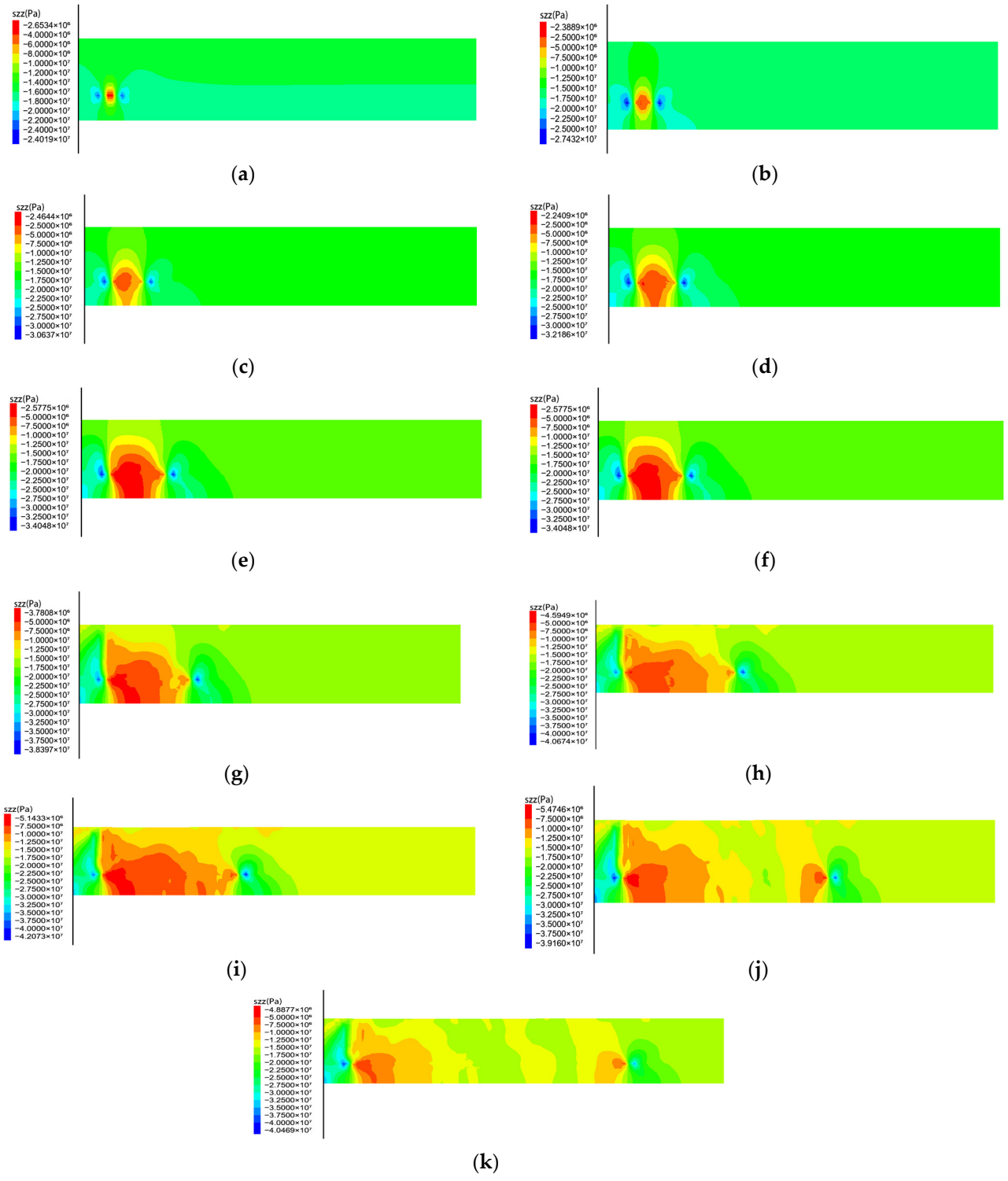

Figure 10. Coal seam mining different distance vertical stress nephogram. (**a**) 10 m. (**b**) 20 m. (**c**) 30 m. (**d**) 40 m. (**e**) 50 m. (**f**) 60 m. (**g**) 80 m. (**h**) 100 m. (**i**) 120 m. (**j**) 180 m. (**k**) 240 m.

In Figure 10a–i, with the increase in the advancing distance, the high vertical stress area always appeared in front of the working face. In addition, the maximum value of the high stress area gradually increases, indicating that the failure range of the overburden rock gradually expands, which shows that mining has a great influence on vertical stress distribution.

By extracting the vertical stress data under different propulsion distances in Figure 11, the vertical stress curves under different propulsion distances can be obtained, as shown in Figure 11. Before the first square of the working face (0~120 m range), with the increase in the advance distance, the peak stress gradually increases from 22.3 MPa to 37.6 MPa, indicating that the larger the advance distance the easier the plastic failure occurs, and the stress concentration area gradually increases. When the advancing distance increases to 180 m (1.5 times the length of the working face), the peak stress decreases to 34.3 MPa. When advancing to 240 m (the length of the working face is 2 times), the peak stress of the advance abutment pressure is reduced to 33.9 MPa.

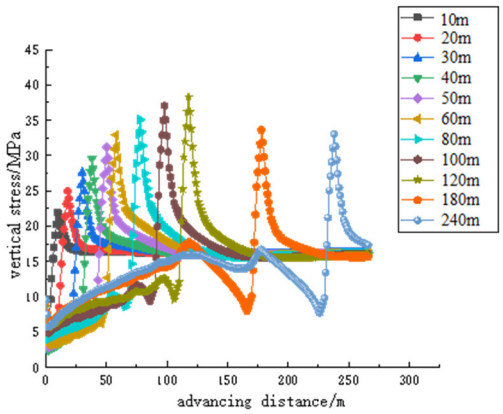

Figure 11. Vertical stress curves at different distances.

To sum up, before the first square of the working face, with the increase in the advancing distance, the peak stress and its influence range are larger. Thus, the more serious the mine pressure near the working face is, the more attention should be paid to the advanced support; when the advancing distance exceeds the length of the working face, the overburden rock falls more fully, and the peak stress decreases slightly, indicating that the failure zone height reaches the maximum.

(2) Plastic failure characteristic under different advancing distances

To reveal the relationship between advancing distance and plastic failure field, the plastic failure characteristics of surrounding rock under different advancing distances are analyzed, as shown in Figure 12. With the increase in advancing distance, the plastic zone of the stope gradually increases. In especial, when the distance is half of the length of the working face, the plastic zone increases rapidly, and the plastic failure zone is slightly larger. At the same time, the plastic zone also develops to both of roof and floor, but the transmission degree of the roof is slightly larger than the floor.

Before the first square of the working face, the development range of the plastic zone shows an evident increasing trend. When the working face advances to 60 m (half of the length of the working face), the height of the plastic zone reaches about 30 m. With the further increase in the advancing distance, the range of the plastic zone further expands. When the working face advances 120 m, that is, when the working face is first squared, the height of the plastic zone reaches a maximum of 40 m. With the further increase in the advancing distance, the development range of the plastic zone increases, and the height remains unchanged.

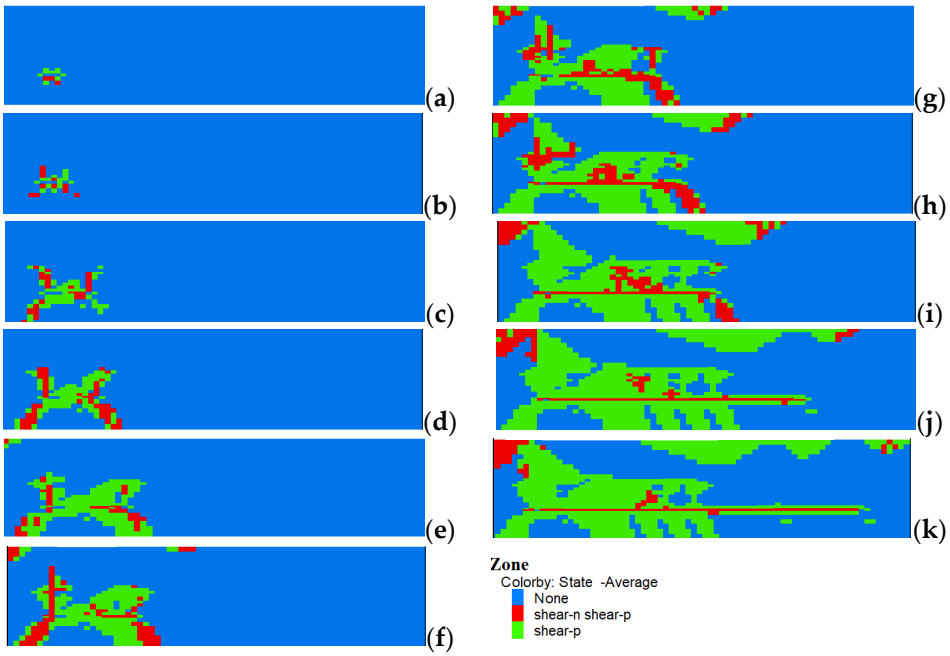

Figure 12. Plastic zone of surrounding rock under different advancing distances. (**a**) 10 m. (**b**) 20 m. (**c**) 30 m. (**d**) 40 m. (**e**) 50 m. (**f**) 60 m (half the length of the working face). (**g**) 80 m. (**h**) 100 m. (**i**) 120 m (the length of the working face). (**j**) 180 m. (**k**) 240 m.

4. Study on Stress Transfer of Overlying Strata in Deep Goaf

4.1. Stope Stress Transfer Model Based on Overlying Strata Movement State of Goaf Boundary

The stress state of the stope is usually complex, and its vertical stress and horizontal stress are related to the distribution of the rock strata. In particular, the horizontal stress is greatly affected by the geological structure. Therefore, it is extremely important to master the stress distribution of the stope to control the stability. After entering deep mining, the vertical stress increases evidently, and the activity range of overlying strata increases, leading to an increase in stress concentration degree of rock strata, thereby affecting the stability of surrounding rock. The increase in rock load leads to the transfer of stress to the stope, and the horizontal stress significantly increases. The fracture development of the rock strata is well correlated to the transfer and release of the horizontal stress. However, the influence of previous related research on horizontal stress is slightly insufficient. Therefore, a stope space model considering the influence of horizontal stress is established, as shown in Figure 13. The model comprehensively considers the mining conditions (such as buried depth, working face length, etc.) and geological conditions (roof lithology, geological structure, rock structure, etc.). The model approximates the horizontal stress as a linear function related to the depth, i.e., the surface horizontal stress is zero, and the horizontal stress gradually increases with mining depth. As the stope space is usually complex, a single model is not easy to precisely reflect the stope stress state. Therefore, scholars mainly use the original rock stress test and stress inversion to obtain more accurate horizontal stress.

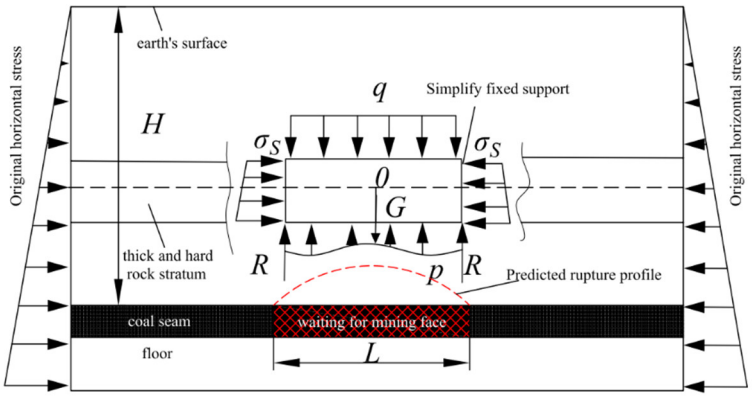

Figure 13. Stope space model considering the influence of horizontal stress.

4.2. Vertical Stress Transfer and Estimation of Overburden in Stope

Figure 14 shows the overburden structure before and after the fracture of thick and hard strata. In Figure 14a, with the increase in the width of the goaf, the rock stratum is broken upward along a certain Angle until it reaches the thick and hard rock stratum, and the breaking height is h_3; the angle between the boundary of the fault rock stratum (the comprehensive overburden fracture line, the black dotted line in the figure) and the horizontal direction is called the overburden fracture angle α; the angle between the connection line of the rock contact point (blue dotted line in the figure) and the horizontal direction is called the overburden contact angle β; the thickness of the thick hard rock to the surface is h_1; the height of the thick hard rock is h_2; the width of the working face to be mined is D; the distance between the fracture points under the thick and hard rock is called the limit step a; at this time, the load is the transfer load of the suspended roof, which is characterized by the insufficient drop of the fractured rock stratum at the boundary of the goaf. Under the horizontal stress, the hinge structure is formed, and the gravity of the rock strata is transferred to both sides, while the rock stratum in the middle of the goaf drops evenly and fully, and the load is all on the gangue. If the overlying strata movement causes the upper roof thick and hard rock stratum to break (Figure 14b), the broken thick and hard rock blocks are interlocking with each other, forming a high-level hinged balance structure. Due to the large fracture height, the formed rotation angle is small, and the load is transferred by the hinges. The characteristics are that the rock load is transferred to one side of the coal and rock mass and the other side of the gangue on average. Additionally, the magnitude of the transferred stress depends on the shape of the thick and hard rock stratum.

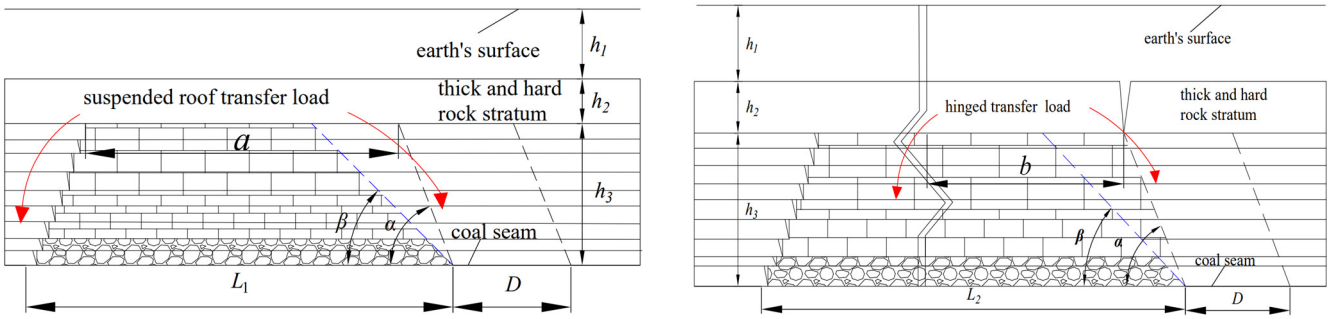

Figure 14. Overburden structure before and after thick hard rock breaking. (**a**) Thick and hard rock strata not broken. (**b**) Thick and hard rock strata broken.

The first mining face is in situ stress state before mining. Without considering the influence on geological structure, the average static vertical stress $\overline{\sigma}_0$ (or in situ stress state) before mining is expressed as

$$\overline{\sigma}_0 = \sum_{i=1}^{n} \gamma_i h_i = \gamma_1 h_1 + \gamma_2 h_2 + \gamma_3 h_3 = \gamma H \tag{11}$$

where γ_1, γ_2, and γ_3 are the average bulk density of each rock group; and H is buried depth.

Through analysis, the thick and hard rock stratum of the mining roof in a small range is a suspended structure. With the mining of the working face, the goaf increases, and the thick and hard rock stratum of the roof changes to a suspended roof structure. To simply the study, the thick and hard rock stratum breaks before reaching the maximum suspended length. At this time, the suspended roof transfer load Q_1 is transferred to the rock mass on both sides on average. The low hinged rock stratum (block) gravity meter between the fracture line and the contact gangue line is Q_2, and the total overburden load transferred to one side of the coal rock mass Q' is obtained:

$$Q' = \frac{Q_1}{2} + \frac{Q_2}{2} = \frac{a(\lambda_1 h_1 + \lambda_2 h_2)}{2} + \frac{\lambda_3 h_3^2(\cot\beta - \cot\alpha)}{4} \tag{12}$$

When the hanging length of thick and hard rock reaches the limit step, then begins to break. After the fracture, the rock load is transferred to the goaf and the other side of the coal and rock mass on average. At this time, half of the hinged load Q_1' of the thick and hard rock block and the low hinged rock layer gravity meter between the fracture line and the contact line are Q_2, which together constitute the load Q'' transferred to the unmined coal and rock mass, i.e., the load Q'' of the coal and rock mass is transferred to the unmined coal and rock mass.

$$Q'' = \frac{Q_1'}{2} + \frac{Q_2}{2} = \frac{b(\lambda_1 h_1 + \lambda_2 h_2)}{2} + \frac{\lambda_3 h_3^2(\cot\beta - \cot\alpha)}{4} \tag{13}$$

4.3. Vertical Stress Transfer Characteristics of Stope

With the extraction of the coal body, the roof and floor boundary of the goaf roof loses its constraint, and the original stress equilibrium state is destroyed. To seek a new mechanical equilibrium state, the overburden stress of the goaf roof is transferred to the goaf, resulting in the increase in the bearing body pressure, thus forming a bearing pressure increase zone, as shown in Figure 15.

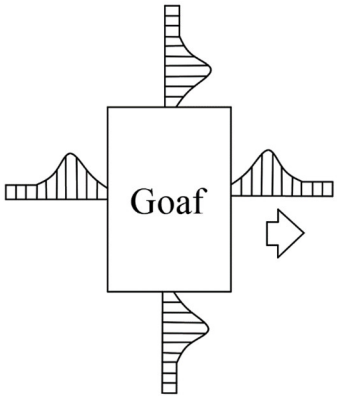

Figure 15. Stress distribution around goaf.

To further explain the reason of working face advancing on overburden pressure transfer and facilitate intuitive analysis, the characteristics of stress transfer are analyzed by advancing 25 m (initial weighting step), 40 m (periodic weighting step 15 m), 55 m, 70 m, 85 m, 120 m (the first square of working face), 160 m, 240 m (the second square of

working face), and the characteristics of stress transfer at different distances of working face advancing are obtained, as shown in Figure 16.

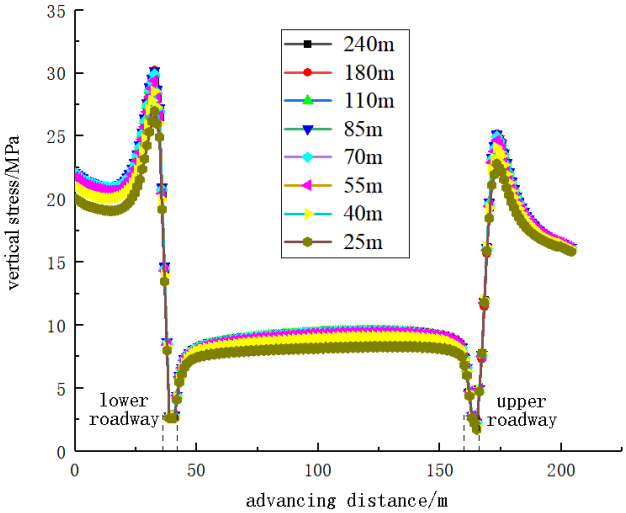

Figure 16. Working face advancing different distance stress transfer characteristics.

With the increase in the advancing distance, the stress is transferred to the surrounding area of the goaf, and the magnitude and range of the stress transfer are different. In addition, the peak stress generally shows an increasing trend, and the scope of the influence is getting larger and larger. The abutment pressure of the solid coal side of the gob-side roadway also generally shows an increasing trend. In general, the stress of the surrounding rock in front of the working face and the solid coal side of the gob-side roadway is large, which should be the key control area of the surrounding rock.

In the range of 0~30 m in front of coal wall, the advance abutment stress increases first and then decreases. The position of peak stress is 4 m from coal wall, and the value is 39.9 MPa, indicating that this stage is greatly affected by the mining activity, and the side roadway of the goaf should be strengthened. The distance from the coal wall is more than 30 m, and the advance abutment stress tends to be gentle. It shows that mining has little effect on the surrounding rock starting from this position.

In a range 0~15 m away from the coal wall behind the working face, the goaf roof beam movement is strong due to the influence of advanced mining. Additionally, the goaf roof appears the phenomenon of rapid stress unloading, indicating that the goaf roof is broken and collapsed at this stage, but the collapsed gangue at this stage is not filled with the goaf. The bending and sinking of the overlying rock beam do not affect the collapsed gangue in the goaf. With the increase in the distance from the coal wall, the abutment stress of the goaf first decreases to the minimum and then increases, indicating that the caving gangue fills the goaf space and then gradually compacts, supporting the overlying rock beam; thus, the stress gradually increases.

From Figure 17, the peak value and spread range of the abutment stress on the solid coal side of the lower roadway are significantly larger than the upper, which is resulted from the dip angle of the coal seam. In the inclined direction, the range of 0~20 m from the coal side of the roadway, the solid coal stress increases. With the further increase in the distance, i.e., when it is greater than 20 m, the abutment stress tends to be fixed and close to the original rock stress.

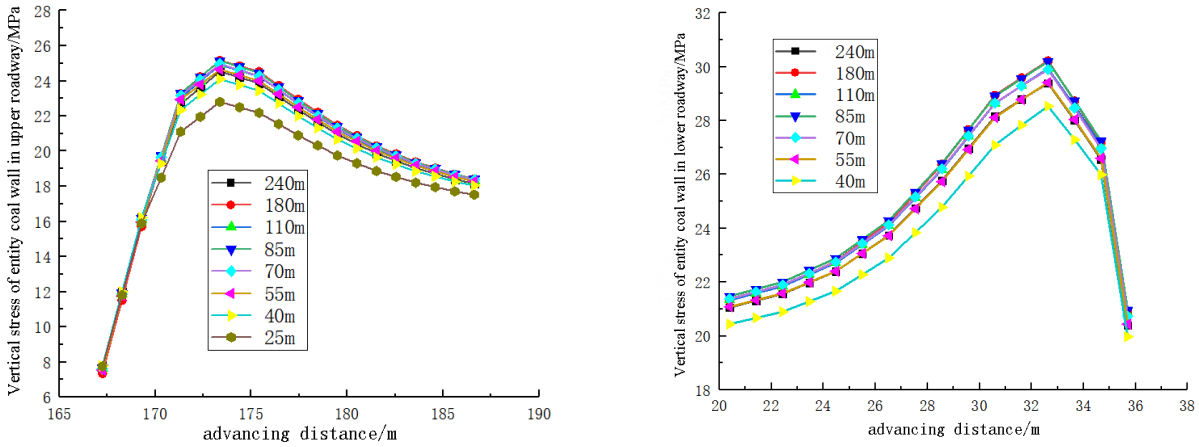

(**a**) (**b**)

Figure 17. Distribution characteristics of abutment stress of solid coal side in gob-side roadway. (**a**) Upper roadway. (**b**) Lower roadway.

The peak stress value and position data of abutment stress under different advancing distances are extracted to obtain Table 2.

Table 2. Peak value and position of lateral abutment pressure of solid coal.

Working Face Advanced Distance/m	Distance from Peak Position to Roadway Side/m		Peak Value/MPa		Stress Concentration Factor	
	Upper Roadway	Lower Roadway	Upper Roadway	Lower Roadway	Upper Roadway	Lower Roadway
25	9.2	3.4	22.80	26.99	1.45	1.63
40	9.2	3.4	24.10	28.53	1.53	1.72
55	9.2	3.4	24.64	29.41	1.56	1.78
70	9.2	3.4	24.96	29.90	1.58	1.81
85	9.2	3.4	25.14	30.20	1.60	1.82
120	9.2	3.4	24.92	29.93	1.58	1.81
180	9.2	3.4	25.16	30.22	1.60	1.82
240	9.2	3.4	24.53	29.39	1.56	1.77

From Table 2, the advancing distance is from 0 to 85 m, and the stress is transferred to the solid coal side of the gob-side roadway, which is caused by the increasing area of the suspended roof in the goaf. With the further increase, the overburden stress in the goaf fluctuates in a small range, which is caused by the further fracture of the goaf roof and the gradual compaction of the goaf gangue. The peak stress position of the solid coal side of the lower roadway is 3.4 m from the roadway side, and the upper roadway is 9.2 m. However, the peak stress value of the lower roadway is evidently larger than that of the upper, which is resulted from the dip angle of the coal seam. This shows that the greater the dip angle of the coal seam, the more evident the stress concentration area of the lower roadway, the more difficult the control. In addition, the stress concentration area of the upper roadway is weaker than the upper roadway. For inclined coal seams, the greater the dip angle the more likely the gangue is to slip, and more reasonable gangue retaining measures should be formulated.

5. "Migrate-Transfer-Control" Technology of Roadway Surrounding Rock and Its Application Effect

5.1. "Migration-Transfer-Control" Technology of Roadway Surrounding Rock

After the excavation of the roadway, the original equilibrium state is destroyed, and the surrounding rock stress is redistributed, as shown in Figure 18. During stress redistribution, part of the stress is released along the excavation face in the form of rebound deformation, and the other part is transferred to the deep roadway surrounding rock. Therefore, the stress is distributed in a gradient. From the stress point of view, it can be divided into a stress reduction zone, stress increase zone, and original rock stress zone. Due to the existence of stress gradient, the fracture degree along the radial direction of roadway is different. Finally, the roadway from shallow to deep forms the fracture zone, plastic zone, and elastic zone successively.

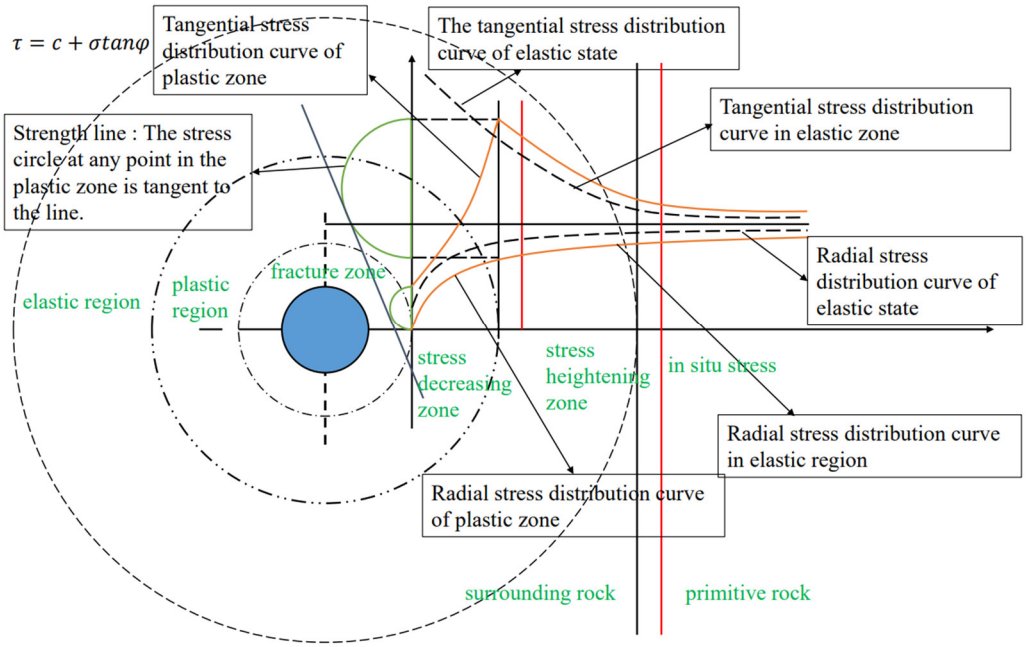

Figure 18. Elastic–plastic deformation zone and stress distribution of surrounding rock of circular roadway [31].

Figure 19 is a simplified mechanical model of a circular roadway. In this model, the vertical stress p_0 and the horizontal stress λp_0 are not equal. It can be considered as the superposition of uniform stress field and horizontal tension vertical compression stress field.

According to elastic mechanics, the stress solution of circular roadway is:

$$\sigma_r = \frac{(1+\lambda)p_0}{2}(1-\frac{R_0^2}{r^2}) - \frac{(1-\lambda)p_0}{2}(1-4\frac{R_0^2}{r^2}+3\frac{R_0^4}{r^4})\cos 2\theta \quad (14)$$

$$\sigma_\theta = \frac{(1+\lambda)p_0}{2}(1+\frac{R_0^2}{r^2}) + \frac{(1-\lambda)p_0}{2}(1+3\frac{R_0^4}{r^4})\cos 2\theta \quad (15)$$

$$\tau_{r\theta} = \frac{(1-\lambda)p_0}{2}(1+2\frac{R_0^2}{r^2}-3\frac{R_0^4}{r^4})\sin 2\theta \quad (16)$$

where σ_r, σ_θ, and $\tau_{r\theta}$ are radial stress, tangential stress, and shear stress, MPa; λ is the lateral pressure coefficient; p_0 is vertical stress, MPa; r_0 is the radius of roadway, m; r is the distance from any point to the center of the roadway, m; and θ is the angle between the line from any point to the center of the roadway and the horizontal x-axis.

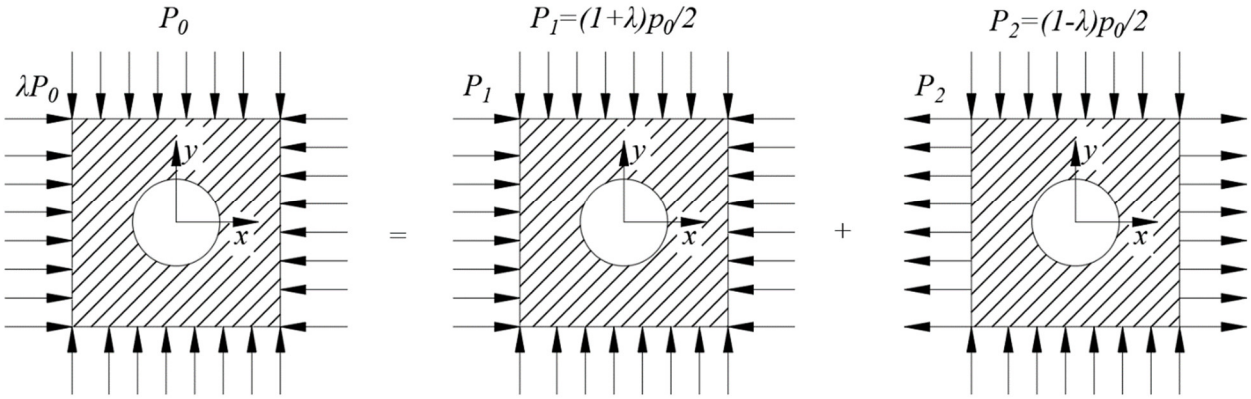

Figure 19. Simplified mechanical model of circular roadway.

Figure 20 is a schematic diagram of the "Migrate-Transfer-Control" technical system in the deep roadway. After roadway excavation, the initial equilibrium state of roadway is broken, the overburden rock moves, the stress is transferred and adjusted, and, finally, the fracture zone, plastic zone, and elastic zone are formed. The strength in fracture zone and plastic zone is greatly lower than that in initial stress state. Therefore, it is crucial to strengthen the control of the fracture and plastic zones. Under normal circumstances, stability needs to be controlled by means of support so that the roadway stress can be restored to the state before excavation as far as possible and the roadway can also reach a safe state.

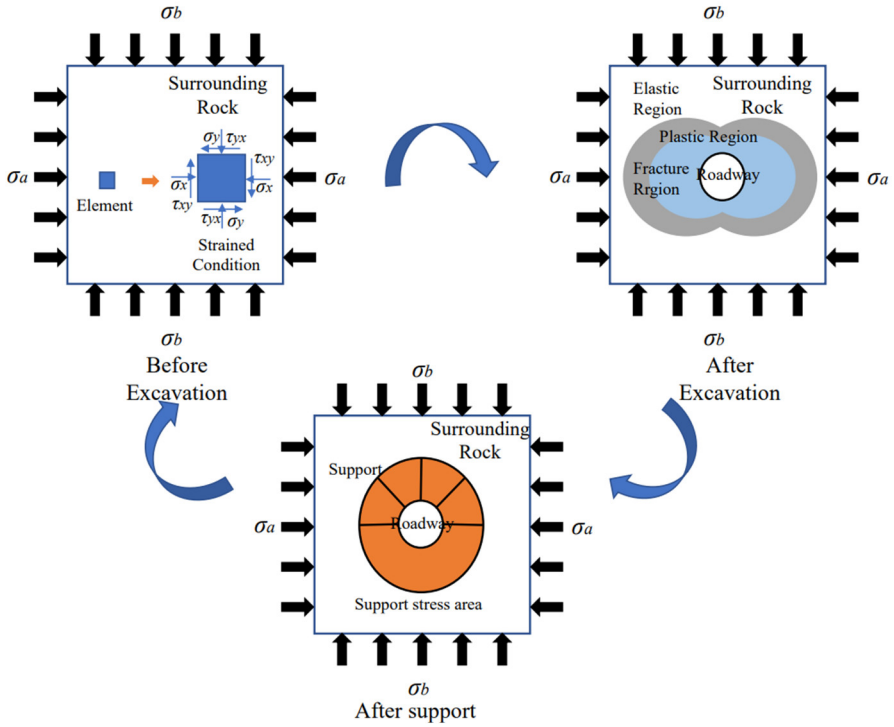

Figure 20. Schematic diagram of "Migrate-Transfer-Control" technology system in deep roadway.

5.2. Roadway Support Scheme Optimization Design and Simulation Analysis

5.2.1. Support Design

Different support schemes are designed for comparative simulation research. On the basis of the original support scheme, the support strength of the roof and the sidewall is strengthened. Three support schemes are designed, namely, the roof strengthening support scheme, the sidewall strengthening support scheme, and the roof and sidewall

strengthening support scheme. The support scheme is shown in Figure 21. FLAC is used for simulation calculation, and the vertical stress and displacement of roadway surrounding rock under different support schemes are compared and analyzed, so as to obtain the optimal support scheme. In the simulation, the anchor rod and anchor cable are cable units, and the parameters are shown in Table 3.

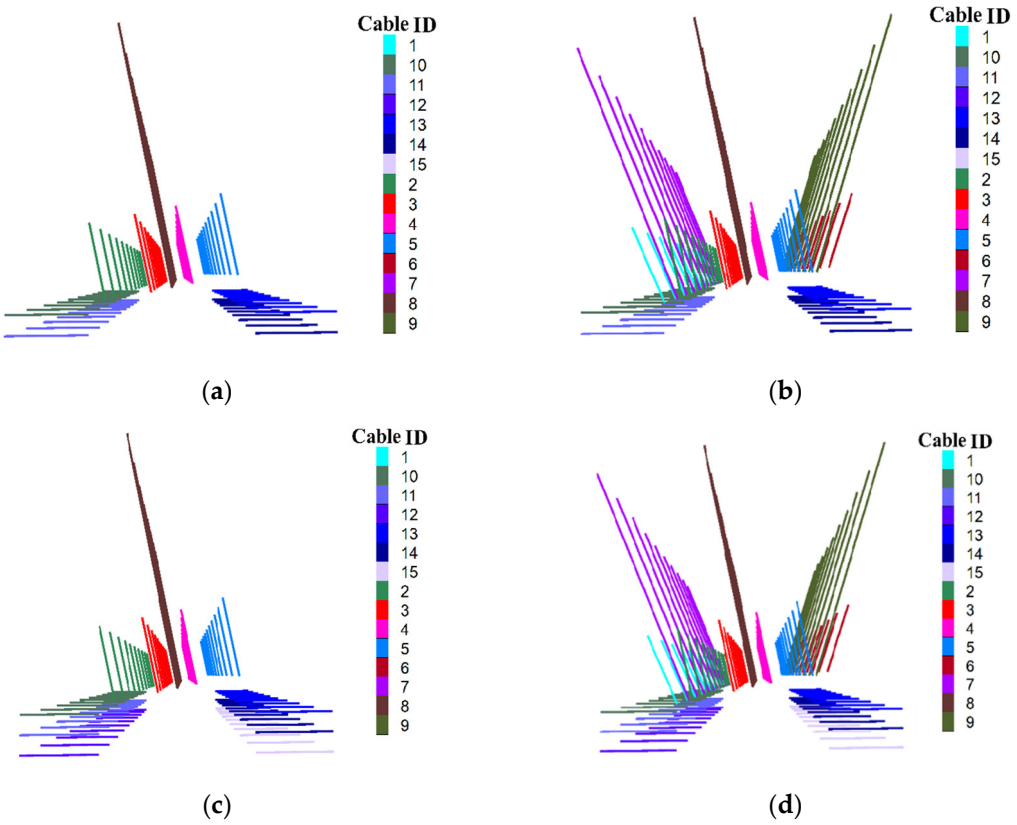

Figure 21. Schematic diagram of different support schemes. (**a**) The original support scheme. (**b**) Roof strengthening support scheme. (**c**) Strengthening support scheme of sidewall. (**d**) Strengthening support scheme of roof and sidewall.

Table 3. Supporting parameters.

Supporting Parts	ID	Diameter/mm	Length/mm	Preload/kN	Elastic Modulus/GPa
Roof bolt	1, 2, 3, 4, 5, 6	20	2000	60	200
Roof anchor cable	7, 8, 9	21.6	6700	50	200
Wall side bolt	10, 11, 12, 13, 14, 15	20	2000	60	200

5.2.2. Simulation Analysis of Supporting Effect

Figure 22 shows the vertical stress cloud diagram of different support schemes. When the scheme is the original support, the maximum vertical stress of the roadway reaches 26.23 MPa. When the roof is strengthened, the maximum vertical stress is 24.67 MPa, which is 5.94% lower than the original support scheme. When the sidewall is strengthened, the maximum vertical stress of the roadway is 25.19 MPa, which is lower by 3.96%. When both the roof and sidewall are strengthened, the maximum vertical stress of the roadway is 22.77 MPa, which is lower by 13.19%.

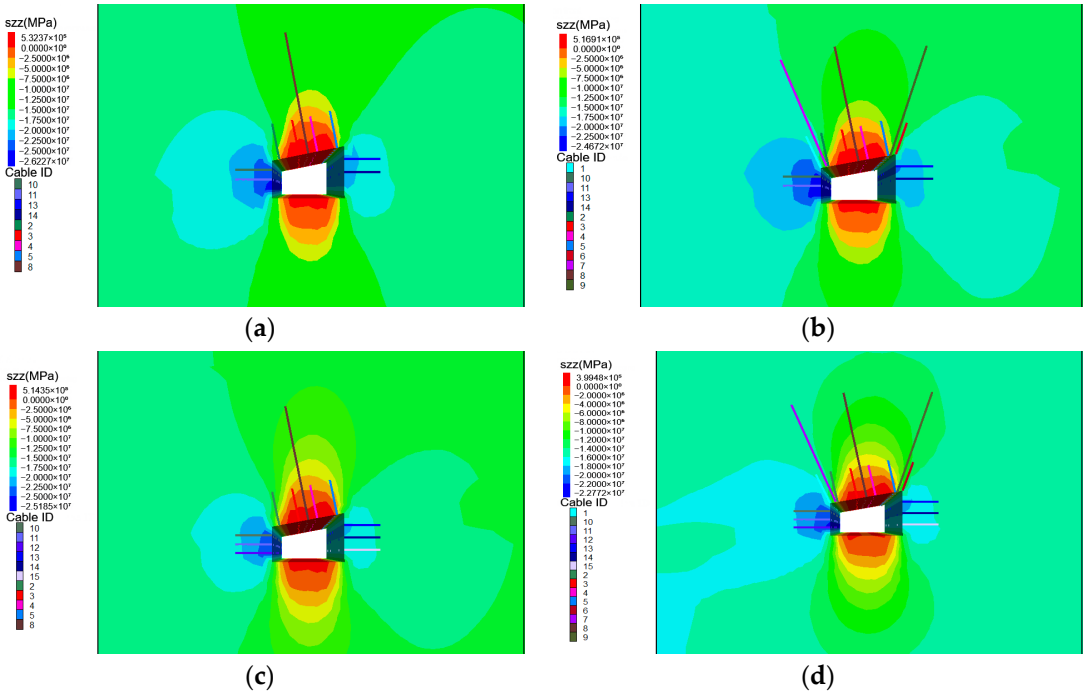

Figure 22. Vertical stress cloud diagram of different support schemes. (**a**) The original support scheme. (**b**) Roof strengthening support scheme. (**c**) Strengthening support scheme of sidewall. (**d**) Strengthening support scheme of roof and sidewall.

Figure 23 shows the vertical displacement cloud diagram of different support schemes. When the scheme is the original support, the maximum subsidence can reach 94 mm. When the roof is strengthened, the maximum subsidence is 63 mm, which is 33.0% lower than the original support scheme. When the sidewall is strengthened, the maximum roof subsidence of the roadway is 66 mm, which is less by 29.8%. After strengthening both the roof and sidewall, the maximum roof subsidence of the roadway is 50 mm, which is less by 46.8%.

Based on the above, after strengthening the roof, the effect of deformation control is slightly greater than that of strengthening the support of the sidewall. The effect of strengthening the support of both the roof and sidewall is undoubtedly the best, and the effect of deformation control is much greater than that of a single factor. Therefore, for deformation control, the roof support should be strengthened first, and then the support of the sidewall. Improving the overall strength is the most effective way to control the deformation of the roadway.

5.3. Roadway Surrounding Rock Field Monitoring and Effect Evaluation

To obtain the law of mine pressure in the working face and verify the rationality of the support scheme, the cross-point method is used to monitor the surface displacement of the roadway to judge the reliability of the support scheme. The displacement curve of the surrounding rock during the mining period is shown in Figure 24.

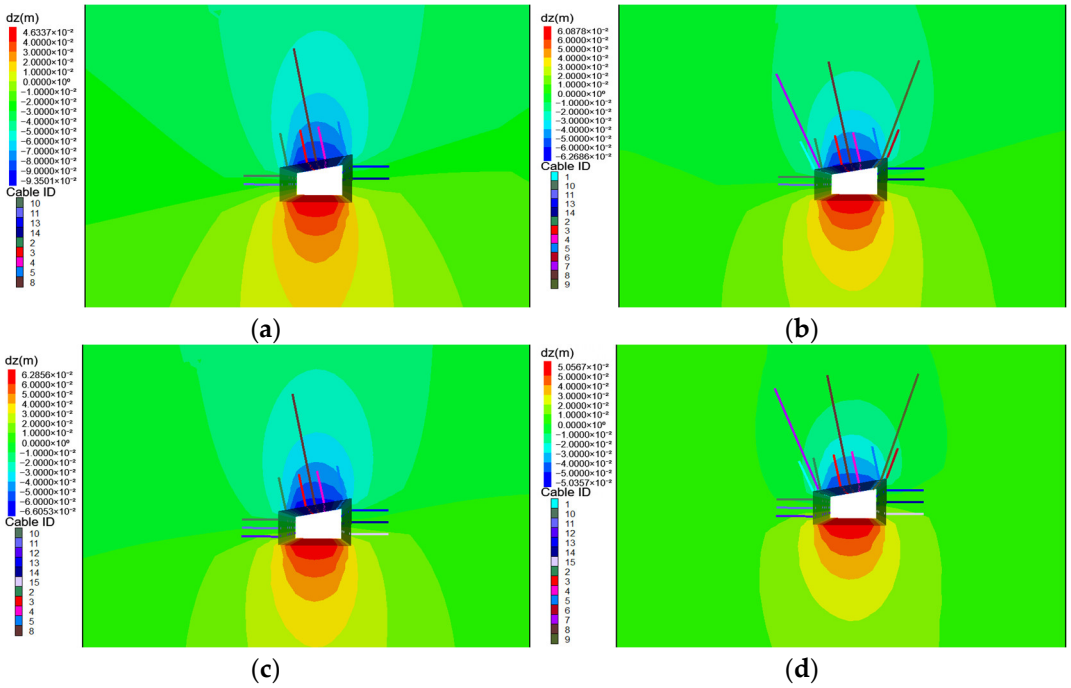

Figure 23. Vertical displacement cloud diagram of different support schemes. (**a**) The original support scheme. (**b**) Roof strengthening support scheme. (**c**) Strengthening support scheme of sidewall. (**d**) Strengthening support scheme of roof and sidewall.

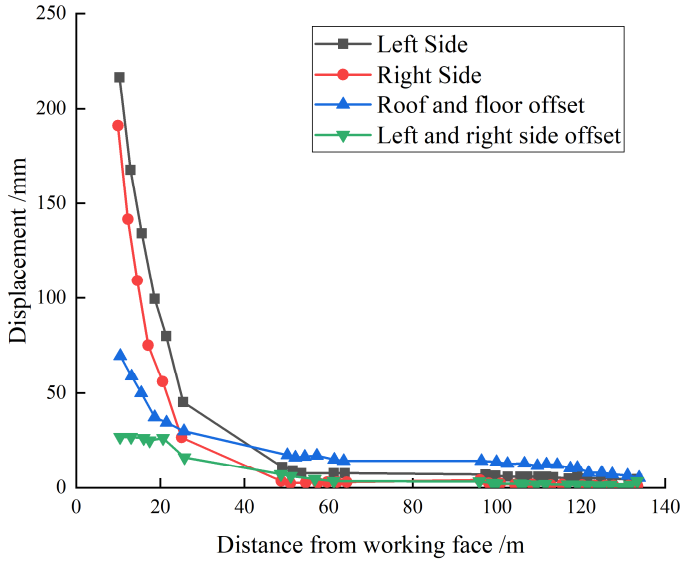

Figure 24. Displacement variation curve of roadway surrounding rock during mining period.

When the measuring point is arranged at a distance greater than 90 m from the working face, the convergence of the two sides of the roadway is 10 mm, and the roof subsidence is 18 mm. The displacement of the surrounding rock changes little. When the advancing distance is constantly approaching the measuring point, the displacement of the two sides is also increasing. When the measuring point is less than 50 m, the deformation of the surrounding rock increases significantly, i.e., the maximum deformation rate of the roof, floor, left side, and right side is 22 mm/d, 12 mm/d, and 9 mm/d, respectively. The reason for the displacement of the two sides is that both of the sides are rapidly deformed, the right side is relatively stable, and the roof subsidence can reach 70 mm. In summary, the change in roof subsidence is small, the left side is the largest, and the right side is small.

6. Discussion

(1) There are some deficiencies in the discussion of the migration law of the overlying strata in goaf. If the size of the established numerical model is small, the discussion on the evolution law of the plastic zone of the surrounding rock of the stope is not accurate enough, which can only reflect the change trend, and a large model should be established for quantitative analysis. In addition, the lack of discussion on the deformation law of overlying rock can be combined with the key layer theory and discrete element numerical simulation software to analyze the displacement law of roof strata. In case of the lack of corresponding field monitoring data, an appropriate amount of field monitoring data should be added for mutual verification.

(2) The stope space model considering the influence of horizontal stress established in this paper can reflect the change in horizontal stress and the movement law of overlying strata, but it only considers the "dynamic load "stress prediction and estimation along the inclined direction of goaf and does not involve the impact induced by the fracture movement of overlying strata. A three-dimensional model should be established based on in situ stress tests.

(3) The analysis of the numerical simulation results of the optimization of the roadway surrounding rock support scheme is not deep enough. Only the vertical stress and vertical displacement of the surrounding rock are compared and analyzed. The overall stress transfer, plastic zone change, and surrounding rock deformation should be comprehensively analyzed. In addition, the supporting length and spacing distance of roadway surrounding rock should also be taken into account, and the integrity of surrounding rock is an important influencing factor of roadway support.

7. Conclusions

(1) Based on the theory of overlying rock failure and instability, the evolution process of overlying rock stress and plastic zone in the advancing process of working face is analyzed by numerical simulation. The results show that the vertical stress and plastic failure range of the surrounding rock in front of the working face increase evidently with the increase in advancing distance of the working face. When the working face advances to the first square, the vertical stress peak and plastic failure height of the surrounding rock in front of working face reach the maximum.

(2) The spatial model of stope considering the influence of horizontal stress is established, and the stress transfer characteristics of overlying strata in stope are analyzed by combining the key stratum theory. It is known that 0~30 m in front of the coal wall of the working face is the influence range of the advanced abutment pressure, and the influence of the mining dynamic pressure in this range is great. The inclined direction of the working face, 0~20 m away from the coal wall of the roadway, is the influence range of the solid coal abutment pressure.

(3) The "Migrate-Transfer-Control" technical system of roadway was proposed and applied to field practice. The field monitoring results show that the displacement variation in the surrounding rock surface of the roadway is smaller when the distance from the working face is greater than 90 m, i.e., the displacement of the two sides is 10 mm, and the roof subsidence is 18 mm; the deformation rate of surrounding rock increases significantly within 50 m from the working face, i.e., the maximum deformation rates of roof and floor, left side, and right side are 22 mm/d, 12 mm/d, and 9 mm/d, respectively.

Author Contributions: Conceptualization, T.Q.; validation, Y.D.; formal analysis and investigation, B.D., Y.N., and T.Q.; data curation, Y.D., B.D., and X.H.; visualization, Y.D.; writing—original draft preparation, Y.D., Y.N. and P.M.; writing—review and editing, Y.D., B.D., and Y.Y.; supervision, T.Q. All authors have read and agreed to the published version of the manuscript.

Funding: This work was supported by the Scientific and Technological Key Project of "Revealing the List and Taking Command" in Heilongjiang Province (2021ZXJ02A03, 2021ZXJ02A04) and the Natural Science Foundation of Heilongjiang Province (LH2019E085).

Institutional Review Board Statement: Not applicable.

Informed Consent Statement: Not applicable.

Data Availability Statement: Not applicable.

Conflicts of Interest: The authors declare no conflict of interest.

References

1. Yuan, L. Scientific conception of precision coal mining. *J. China Coal Soc.* **2017**, *42*, 1–7. [CrossRef]
2. Yuan, L. Research progress of mining response and disaster prevention and control in deep coal mines. *J. China Coal Soc.* **2021**, *46*, 716–725. [CrossRef]
3. Yuan, L. Strategic thinking of simultaneous exploitation of coal and gas in deep mining. *J. China Coal Soc.* **2016**, *41*, 1–6. [CrossRef]
4. Li, C.C. Rock Support Design Based on the Concept of Pressure Arch. *Int. J. Rock Mech. Min. Sci.* **2006**, *43*, 1083–1090. [CrossRef]
5. Xie, H.P.; Zhou, H.W.; Xie, D.J.; Wang, H.W.; Zhang, R.; Gao, F. Research and consideration on deep coal mining and critical mining depth. *J. China Coal Soc.* **2012**, *37*, 535–542. [CrossRef]
6. Qian, M.G. A Structural Model of Overlying Strata in Longwall workings and its Application. *J. China Inst. Min. Technol.* **1982**, *2*, 6–16.
7. Qian, M.G. Review of the Theory and Practice Control Around Longwall Face in Recent 20 Years of Strata. *J. China Univ. Min. Technol.* **2000**, *1*, 1–4.
8. Qian, M.G.; Zhang, D.L.; Li, L.J.; Kang, L.X.; Xu, J.L. "S-R" Stability for the Voussoir Beam and Its Application. *Mine Press. Roof Manag.* **1994**, *3*, 6–11.
9. Qian, M.G.; Miao, X.X.; He, F.L. Analysis of key block in the structure of voussoir beam in longwall mining. *J. China Coal Soc.* **1994**, *6*, 557–563. [CrossRef]
10. Li, Q.; Guo, J.; Zhang, C.; Yang, Y.; Ma, J.; Ren, Z. Research Findings on the Application of the Arch Structure Model in Coal Mining, a Review. *Sustainability* **2022**, *14*, 14714. [CrossRef]
11. Qian, M.G.; Xu, J.L. Behaviors of strata movement in coal mining. *J. China Coal Soc.* **2019**, *44*, 973–984. [CrossRef]
12. Xu, J.L.; Qian, M.G.; Zhu, W.B. Study on Influences of Primary Key Stratum on Surface Dynamic Subsidence. *Chin. J. Rock Mech. Eng.* **2005**, *5*, 787–791.
13. Xu, J.L.; Qian, M.G. Study on the influence of key strata movement on subsidence. *J. China Coal Soc.* **2000**, *2*, 122–126. [CrossRef]
14. Miao, X.X.; Chen, R.H.; Pu, H.; Qian, M.G. Analysis of Breakage and Collapse of Thick Key Strata around Coal Face. *Chin. J. Rock Mech. Eng.* **2005**, *8*, 1289–1295.
15. Kong, L.H. Overlying strata movement law and its strata pressure mechanism in fully mechanized top-coal caving workface with large space. *J. Min. Saf. Eng.* **2020**, *37*, 943–950. [CrossRef]
16. Kuang, T.; Li, Z.; Zhu, W.; Xie, J.; Ju, J.; Liu, J.; Xu, J. The Impact of Key Strata Movement on Ground Pressure Behaviour in the Datong Coalfield. *Int. J. Rock Mech. Min. Sci.* **2019**, *119*, 193–204. [CrossRef]
17. Li, Z.; Xu, J.; Ju, J.; Zhu, W.; Xu, J. The Effects of the Rotational Speed of Voussoir Beam Structures Formed by Key Strata on the Ground Pressure of Stopes. *Int. J. Rock Mech. Min. Sci.* **2018**, *108*, 67–79. [CrossRef]
18. Dong, F.T.; Song, H.W.; Guo, Z.H.; Lu, S.M.; Liang, S.J. Roadway Support Theory Based on Broken Rock Zone. *J. China Coal Soc.* **1994**, *1*, 21–32.
19. Hou, C.J.; Gou, P.F. Mechanism Study on Strength Enhancement for the Rocks Surrounding Roadway Supported by Bolt. *Chin. J. Rock Mech. Eng.* **2000**, *3*, 342–345.
20. Fang, Z.L. *Characteristics of Tension and Compression Area and Maintenance Theory of Primary and Secondary Bearing Area*; Soft Rock Engineering Committee of Chinese Society of Rock Mechanics and Engineering, Coal Mine Soft Rock Engineering Technology Research and Extension Center: Beijing, China, 1999; pp. 58–61.
21. Qin, X.M.; Hao, F.K. *Soft Rock Composite Support Technology of Ronghua Shaft*; Soft Rock Engineering and Deep Disaster Control Branch, Chinese Society of Rock Mechanics and Engineering: Beijing, China, 2009; pp. 193–195.
22. Xie, Z.; Zhang, N.; Yuan, Y.; Xu, G.; Wei, Q. Study on Safety Control of Composite Roof in Deep Roadway Based on Energy Balance Theory. *Sustainability* **2019**, *11*, 3688. [CrossRef]
23. Wang, C.; Liu, L.; Elmo, D.; Shi, F.; Gao, A.; Ni, P.; Zhang, B. Improved Energy Balance Theory Applied to Roadway Support Design in Deep Mining. *J. Geophys. Eng.* **2018**, *15*, 1588–1601. [CrossRef]

24. Zuo, J.P.; Wen, J.H.; Liu, D.J.; Wu, L.L.; Sun, Y.J. Control theory of uniform strength support in deep roadway. *J. Min. Sci. Technol.* **2021**, *6*, 148–159. [CrossRef]
25. Kang, H.P. Analysis on types and interaction of stress fields in underground coal mines. *J. China Coal Soc.* **2008**, *33*, 1329–1335.
26. Kang, H.P. Seventy years development and prospects of strata control technologies for coal mine roadways in China. *Chin. J. Rock Mech. Eng.* **2021**, *40*, 1–30. [CrossRef]
27. Kang, H.P.; Jiang, P.F.; Yang, J.W.; Wang, Z.G.; Yang, J.H.; Liu, Q.B.; Wu, Y.Z.; Li, W.Z.; Gao, F.Q.; Jiang, Z.Y.; et al. Roadway soft coal control technology by means of grouting bolts with high pressure-shotcreting in synergy in more than 1000 m deep coal mines. *J. China Coal Soc.* **2021**, *46*, 747–762. [CrossRef]
28. Ma, N.J.; Zhao, X.D.; Zhao, Z.Q.; Li, J.; Guo, X.F. Stability analysis and control technology of mine roadway roof in deep mining. *J. China Coal Soc.* **2015**, *40*, 2287–2295. [CrossRef]
29. Zhang, H.; Li, G.S.; Jiang, S.Q. Time-space evolution pattern simulation experiment of surrounding rock deformation and destruction for super kilometer deep shaft roadway. *J. Exp. Mech.* **2018**, *33*, 979–986.
30. Ren, Z.Y. Technology of Bolt and Cable and Bolt- Grouting Coupling Support in Deep High Stress and Soft Rock Roadway. *Coal Sci. Technol.* **2013**, *41*, 30–33+37. [CrossRef]
31. Zhao, G.M.; Xu, W.S.; Meng, X.R.; Liu, C.Y. Instability mechanism of high stress rock mass under excavation and unloading induced by disturbance. *J. China Coal Soc.* **2020**, *45*, 936–948. [CrossRef]

Disclaimer/Publisher's Note: The statements, opinions and data contained in all publications are solely those of the individual author(s) and contributor(s) and not of MDPI and/or the editor(s). MDPI and/or the editor(s) disclaim responsibility for any injury to people or property resulting from any ideas, methods, instructions or products referred to in the content.